Ccq1 restrains Mre11-mediated degradation of short telomeres

Julien Audry
Aix Marseille Univ, CNRS, INSERM, Institut Paoli-Calmettes

Kurt Runge (rungek@ccf.org)
Cleveland Clinic Lerner College of Medicine https://orcid.org/0000-0001-8492-0530

Article

Keywords:

Posted Date: March 24th, 2022

DOI: https://doi.org/10.21203/rs.3.rs-1456395/v1

Ccq1 restrains Mre11-mediated degradation of short telomeres.

Julien Audry[1,*] and Kurt W Runge[1,2,*]

[1] Department of Inflammation and Immunity, Lerner Research Institute, Cleveland Clinic Foundation, Cleveland, Ohio, 44195 USA

[2] Department of Genetics and Genome Sciences, Case Western Reserve University, Cleveland, Ohio, 44106 USA

* Corresponding authors: to Kurt W Runge, rungek@ccf.org and to Julien Audry, audryj@ccf.org

Word count for Abstract:145 words

Word count for Introduction, Results and Discussion: 4,245 words

Word count for Materials and Methods: 1,216 words

Word count for 10 Figure Legends: 2,340 words

Abstract

Telomeres cap chromosome ends with specialized chromatin composed of DNA repeats bound by a multiprotein complex called shelterin. Fission yeast telomeres can be formed by cleaving a "proto-telomere" bearing 48 bp of telomere repeats to form a new stable chromosomal end that prevents the rapid degradation seen at similar DNA double-strand breaks (DSBs). This end-protection was investigated in viable mutants lacking telomere-associated proteins. Telomerase, the shelterin components Taz1, Rap1, or Poz1 or the telomere-associated protein Rif1 were not required to form a stable chromosome end after cleavage of the proto-telomere. However, cells lacking the fission yeast shelterin component Ccq1 converted the cleaved telomere repeat-capped end to a rapidly degraded DSB. Degradation was greatly reduced by eliminating the nuclease activity of Mre11, a component of the Mre11-Rad50-Nbs1/Xrs2 complex that processes DSBs. These results demonstrate a novel function for Ccq1 to effect end-protection by restraining Mre11-dependent degradation.

Introduction

Telomeres are specialized double-strand breaks (DSBs) at chromosome ends that facilitate their replication and prevent DNA degradation and activation of the DNA damage checkpoint (for review: [1–3]). In many eukaryotes, telomeres consist of G-rich repeats synthesized by telomerase to form a tract of double-strand repeats with a 3' single-stranded overhang. Specialized proteins bind to these repeats to form a complex called shelterin, which shows strong evolutionary conservation between mammals and the fission yeast *Schizosaccharomyces pombe* [2,4–6]. The telomere repeats and bound proteins can provide protection of the chromosome end and full replication in yeast and humans [7–9].

In *S. pombe,* the internal telomere repeats are bound by Taz1, which anchors Rap1 and its associated protein Poz1 in what is considered the double-strand binding complex (Fig. 1)(analogous to the TRF1/TRF2-RAP1-TIN2 complex in human shelterin)[3,10]. Taz1 also interacts with Rif1, a protein conserved throughout eukaryotes with roles in telomere length regulation, DNA replication in fungi [10–13] and as a component of the DSB processing regulator Shieldin [14,15]. Deletion of any of these genes in *S. pombe* results in viable cells with elongated chromosomal telomere repeat tracts [10,16–18].

S. pombe telomeres end in a single-stranded 3' DNA overhang bound by Pot1 [19]. Pot1 interacts with Tpz1 and Ccq1, analogous to the mammalian POT1-TPP1 complex, which interact with Poz1 (Fig. 1)[18,20–22] These proteins have important roles in protecting the telomere end from degradation, as cells born without Pot1 eventually die or circularize their chromosomes [19]. Cells lacking Tpz1 have a similar phenotype [18]. The phenotype of cells lacking Ccq1 is more complex. Ccq1 helps recruit telomerase to the telomere via a TQ motif at amino acids 93-94 that is phosphorylated by the ATM kinases Rad3 or Tel1 and promotes

58 interaction with the telomerase subunit Est1 [23–25]. Cells in which Ccq1 has been deleted or
59 the *ccq1-T93A* mutation introduced first slowly shorten their telomere repeats tracts. After many
60 generations (over ~80 doublings), the cells contain either circularized chromosomes or linear
61 ones with very short telomere repeat tracts maintained by a telomerase-independent
62 mechanism [26–28]. Finally, Ccq1 has another role as part of the histone-modifying complex
63 SHREC, which is required for heterochromatin at the telomere and other loci [28,29].
64
65 One challenge in the analysis of telomere protein function and regulation of the length of the
66 telomere repeat tract is the delay between making the mutation and analysis of telomeres.
67 Mutations constructed by transformation or genetic crosses start with cells bearing normal
68 length telomeres which then change during the ~30 generations of growth required to generate
69 sufficient material for analysis of telomeric chromatin. Mutations that convert telomeres to
70 rapidly degraded DSBs are difficult to study with this approach. Consequently, a system that
71 can follow the modification of a short telomere tract in real time can provide additional, important
72 information about the requirements for distinguishing a telomere from an internal chromosomal
73 DSB.
74
75 We recently developed an inducible telomere formation system in *S. pombe* using the I-SceI
76 homing endonuclease [30]. The system uses “proto-telomere” cassettes bearing either a tract
77 of 48 bp of *S. pombe* telomere repeats (named *2R-48 bp*) or a 0 bp (*2R-0 bp*). Induction of
78 transcription of I-SceI induces a DSB to expose the 48 bp telomere sequence at *2R-48 bp* or
79 create a DSB at *2R-0 bp* (Figs. 2A, S1). The cleaved *2R-48 bp* cassette immediately gained
80 telomere function as the end was protected and elongated to a full-length telomere, while the
81 DSB at the *2R-0 bp* cassette was degraded [30]. Consequently, the *2R-48 bp* and *2R-0 bp*
82 proto-telomere system provide a strong model to investigate how telomere-repeat capped ends
83 are distinguished from a DSB.

84

85 Following telomere formation at the cleaved *2R-48 bp* proto-telomere in viable mutants lacking
86 telomerase or telomere-bound proteins revealed a novel function for Ccq1 in distinguishing
87 telomeres from DSBs. The cleaved *2R-48 bp* proto-telomere was rapidly degraded in *ccq1*Δ
88 cells, similar to a DSB. This *ccq1*Δ rapid degradation phenotype was distinct from a *ccq1*
89 mutation that blocked telomerase recruitment but was very similar to a *tpz1* mutation that
90 interferes with Ccq1 recruitment to telomeres. The immediate degradation of the cleaved *2R-48*
91 *bp* telomere in *ccq1*Δ cells was relieved by eliminating the nuclease activity of Mre11, a
92 component of the DNA damage checkpoint complex MRN/X that processes DSBs. Thus, Ccq1
93 prevents Mre11 from stimulating DNA degradation at the newly formed short telomere.

Results

Telomere formation in cells lacking the double-strand DNA binding components of shelterin leads to a constant rate of telomere elongation to longer, steady-state lengths. The inducible telomere formation system consists of the I-SceI endonuclease under the control of an ahTET-inducible promoter proto-telomeres placed 3' to the *gal1*$^+$ locus (Fig. S1)[30]. Inducing I-SceI production results in cleavage of the control *2R-48 bp* telomere after 1 hour (h) followed by addition of telomere repeats to the I-SceI generated end or the 48 bp telomere repeat tract, and reaches steady-state lengths within 8 to 12 h with lengths of ~160 bp of telomere repeats (Fig. 2B)[30]. The distal *hph*$^+$ fragment was detected transiently by Southern blotting, but the signal was very weak by 8 h (Fig. 2B). In contrast, the control *2R-0 bp* proto-telomere with no telomere repeats is rapidly degraded upon cleavage as expected for an induced DSB: hybridization to the ~350 bp *ura4*$^+$ band and the distal *hph*$^+$ DNA fragment was rapidly lost (Fig. 2C,D)[30]. -A DSB induces a cell cycle pause at the G2 until the break is repaired, which can be detected by an increase cell doubling time [31]. A significant increase in doubling time was only observed in *2R-0 bp* cells (Fig. 2E), and their survival required a Rad52-dependent recombination event (Fig. S2)[30], In contrast, the *rad52*Δ *2R-48 bp* cells formed a functional telomere (Fig. S2B). Consequently, a property of the 48 bp of telomere repeats is to protect the cleaved end immediately after I-SceI cleavage, which we refer to as end-protection.

2R-48 bp cleavage after I-SceI induction occurred similarly in wild type, *taz1*Δ, *rap1*Δ and *poz1*Δ cells, with ≥80% proto-telomere cleavage in 4 h (Figs. 3A-C, S3A,B and Table S1). The cleaved *2R-48 bp* telomere was not degraded, and became greatly elongated in the *taz1*Δ*, rap1*Δ*, and poz1*Δ cells over 32 h (Figs. 3A-C, S3A), similar to the chromosomal telomere lengths originally described for these mutants. Comparing telomere elongation in wild type, *taz1*Δ*, rap1*Δ*,* and *poz1*Δ cells revealed that the initial rates for the first 2 h were similar but

119 increased in the mutants 4 h after the induction to form hyper-elongated telomere repeats (Fig.
120 S3D). In contrast, wild type elongation began to slow at 8 h, as telomeres attained their
121 equilibrium length (Fig. S3D). Cell growth rates and viability in uninduced cells and 0-8 or 8-32
122 h after I-SceI induction were indistinguishable (Fig. S3C,E), in contrast to the growth delay
123 previously observed when the *2R-0 bp* proto-telomere is cleaved to form a repairable DSB that
124 activates DNA damage checkpoints (Fig. 2E)[30]. Consequently, loss of Taz1, Rap1, or Poz1
125 did not affect the end protection afforded by the 48 bp telomere tract.
126
127 **Telomere formation in cells lacking Rif1 leads to a biphasic rate of telomere elongation to**
128 **the final steady-state length.**
129 Rif1 has roles in telomere repeat tract length regulation, DNA DSB repair and the timing of DNA
130 origin of replication firing [10–12,32–34], and loss of Rif1 had different effects on telomere
131 formation. *rif1*Δ cells initially showed wild type rates of telomere elongation, followed by a
132 slower rate of elongation that required ~200 h of growth to reach the steady-state telomere
133 length (Figs. 3D, S4A-C). As with *taz1*Δ*, rap1*Δ and *poz1*Δ cells, growth of *rif1*Δ cells after I-
134 SceI induction, colony size and viability were not significantly different from wild type cells (Figs.
135 3E, S4D,E). Therefore, Rif1 was not required to protect the telomere repeat-capped end.
136
137 **The newly formed short telomere is stable in cells lacking active telomerase but**
138 **immediately degraded in cells lacking Ccq1.**
139 Cells lacking telomerase activity, due to loss of telomerase RNA (TER1) or the telomerase
140 component Est1, formed a stable new telomere end that shortened slowly over time but was still
141 detectable at 32 h post-induction (Fig. 4A,B)[30]. Thus, telomerase activity was not required for
142 protection of the telomere repeat-capped end.
143

144 Ccq1 helps recruit telomerase to the telomere [23,25,26], but its loss led to the rapid
145 degradation of the cleaved proto-telomere immediately after the I-SceI induction (Figs. 4C,
146 S5A). The cleaved *ura4*$^{+}$ band became undetectable after ~4 h, similar to the degradation of
147 the same band from the *2R-0 bp* DSB in wild type cells (Fig. 4C vs. Figs. 2C, 4E). *ccq1*Δ cells
148 also showed a significant growth delay at 0-8 h and 8-32 h post-induction (Fig. 4D), mimicking
149 the growth delays observed with the *2R-0 bp* proto-telomere (a DSB)(Figs. 2E,F, 4D, S5B,C
150 [30]). *S. pombe* cells, paused in G2 of the cell cycle, continue to elongate [35], and the *ccq1*Δ
151 *2R-48 bp* cells became significantly longer 8 and 24 h after I-SceI induction (Fig. 4F), consistent
152 with the DNA damage checkpoint activation.
153
154 **Ccq1 and Pot1 are only recruited after cleavage of the proto-telomere.**
155 To test whether the rapid proto-telomere degradation in *ccq1*Δ cells was due to an altered
156 presence of the DNA binding proteins at the telomere repeats in proto-telomere, Taz1, Pot1,
157 and Ccq1 occupancy at the proto-telomere was monitored by chromatin immunoprecipitation
158 (ChIP) before and during telomere formation (Figs. 5, S6). Taz1 was detected near the
159 telomere repeats at similar levels at the *2R-48 bp* proto-telomere in wild type and *ccq1*Δ cells at
160 0 h and 2 h post-I-SceI induction (Fig. 5A), consistent with the established binding of Taz1 to
161 interstitial telomere repeats [16,36,37]. In wild type cells, the Taz1 ChIP signal increased as
162 new telomere repeats were added, while the Taz1 signal was lost from *ccq1*Δ cells as the
163 telomere was degraded (Figs. 5A, S6A). Only background Taz1 signal was detected at the *2R-*
164 *0 bp* DSB control that lacks telomere repeats. Therefore, Taz1 was present before and after I-
165 SceI cleavage but could not prevent the rapid degradation of the cleaved *2R-48 bp* telomere in
166 *ccq1*Δ cells.
167
168 Ccq1 and Pot1 were not detectable until formation of the new telomere end, with the majority of
169 signal adjacent to the telomere repeats and a weaker signal 3 kb from the I-SceI site (Figs.

170 5B,C, S6B,C). No significant recruitment of Pot1 to the new telomere in *ccq1*Δ *pot1-myc 2R-48*
171 *bp* cells was detected, even though the *ura4*$^{+}$-telomere band was detectable at 2 h (Fig. 4C),
172 suggesting that Pot1 was unable to bind the cut proto-telomere prior to its degradation.
173
174 **Degradation of the newly formed short telomere in *ccq1*Δ cells is not rescued by**
175 **increasing *pot1*$^{+}$ gene number.**
176 If Ccq1 was required for efficient Pot1 binding at the cleaved *2R-48 bp* proto-telomere, then
177 Pot1 levels in *ccq1*Δ cells maybe too low to bind the newly formed telomere. In this hypothesis,
178 increasing *pot1*$^{+}$ gene number might provide sufficient Pot1 to prevent degradation of the
179 cleaved proto-telomere in *ccq1*Δ cells. An untagged *pot1*$^{+}$ cDNA was expressed from the strong
180 *nmt1* promoter from a multi-copy, episomal plasmid (Table S2) because epitope tags are known
181 to alter Pot1 function [38,39]. The presence of the Pot1 plasmid did not alter cell growth or I-
182 SceI cleavage in wild type or *ccq1*Δ cells. The newly formed telomere in *ccq1*Δ *2R-48 bp* cells
183 was rapidly degraded in cells bearing the empty vector and the vector expressing Pot1, while
184 cells bearing a positive control vector expressing Ccq1 formed stable telomeres (Fig. S7). The
185 results suggested a more complex role for Ccq1 in protection of telomere repeat-capped ends.
186
187 **Protection of telomere repeat-capped ends does not require active telomerase.**
188 Phosphorylation of Ccq1 at the T93 residue is a major pathway to recruit telomerase to
189 telomeres via the interaction of phosphorylated Ccq1 and the telomerase subunit Est1.
190 Introducing the *ccq1-T93A* mutation causes normal length telomere repeat tracts to shorten
191 over ~80 generations until the repeats are no longer detectable [23–25]. Cells lacking
192 telomerase or both ATM kinase family members, Rad3 and Tel1, have the same phenotype
193 [40], and Rad3 is considered to be the major kinase that phosphorylates Ccq1 T93 [23,25]. To
194 determine whether the presence of long telomere repeat tracts masked *ccq1-T93A* effects on

195 end protection, telomere formation was assayed in *ccq1-T93A* cells and *rad3-D2249A (rad3-kd)*
196 cells that lack Rad3 kinase activity [41,42].
197
198 The *rad3-kd* cells were proficient for end protection of the cleaved *2R-48 bp* proto-telomere, but
199 produced elongated telomere repeat tracts that were shorter than wild type cells (Fig. 6A,C),
200 similar to the chromosomal telomeres in *rad3*$^-$ cells [43,44]. I-SceI induction and proto-telomere
201 cleavage did not significantly change *rad3-kd* cell growth rate and had only small effects on
202 survival (Figs. 6D, S8A,B). Therefore, the elimination of the Rad3 kinase activity did not impact
203 the *2R-48 bp* proto-telomere end protection.
204
205 The *ccq1-T93A* cells were also proficient for end protection as the cleaved 2*R-48 bp* telomere
206 was stable but not elongated and showed some shortening at 24 h (Figs. 6B, S8C), similar to
207 the telomeres in *TER1*Δ or *est1*Δ cells (Fig. 4A,B). At late time points: telomeres in *TER1*Δ and
208 *est1*Δ cell telomere fragments were readily detectable while the *ccq1-T93A* cell telomeres were
209 less intense at 24 h and not detectable at 32 h (Figs. 4A,B, 6B, S8D). The doubling time
210 increase in the 8-32 h period in the *ccq1-T93A* cells was consistent with loss of the telomere, in
211 contrast to *TER1*Δ and *est1*Δ cells (Fig. 6D vs. Fig. 4D).
212
213 After telomerase recruitment, the Tpz1-K75 residue is important for telomerase activation. The
214 *tpz1-K75A* mutation produces cells in which telomerase is at the telomere by ChIP, but
215 telomerase activity is significantly diminished [45]. The telomeres formed in these *2R-48 bp*
216 cells were short and became more heterogeneous with continued growth (Figs.6C, S8E),
217 potentially due to small amounts of lengthening and shortening at the individual telomere in
218 different cells, as observed previously in budding yeast [46]. Therefore, cleavage of the *2R-48*
219 *bp* proto-telomere in *tpz1-K75A* cells did not show an alteration in proto-telomere cleavage,

220 cellular growth or stability of the telomere repeat-capped end (Figs. 6D,E, S8D,E), showing that
221 those cells are proficient for end protection.
222
223 **End protection requires the Ccq1-Tpz1 interaction but not the Ccq1-Clr3 (SHREC)**
224 **interaction**
225 Ccq1 directly interacts with Clr3, the histone deacetylase of the SHREC complex required for
226 heterochromatin at telomeres and elsewhere [28,29,47]. Cells lacking Clr3 were also proficient
227 for end protection and elongation of the cleaved 2*R-48 bp* proto-telomere, and the telomere
228 repeat tracts observed at 8 and 24 h post-induction were slightly shorter than those of wild type
229 cells (Fig. 7A,C,D). Therefore, the ability of Ccq1 to allow cells to distinguish a telomere repeat
230 capped end from a DSB is independent of recruiting SHREC.
231
232 Tpz1 interacts with Ccq1 and is essential for telomere function as cells lacking Tpz1 are inviable
233 unless the telomeres are eliminated by chromosome circularization [18]. The *tpz1-L449A*
234 mutation significantly weakens recruitment of Ccq1, and consequently telomerase, to telomeres
235 [20,27]. Induction of I-SceI cleavage of the 2*R-48 bp* proto-telomere in *tpz1-L449A* cells
236 resulted in a degradation of the *ura4*$^+$ telomere band (Figs. 7B, S9), that was similar to the
237 degradation in *ccq1*Δ cells, with a comparable delay in cell growth (Fig. 7C-right panel, D).
238 Thus, Tpz1 plays an essential role in end protection of the cleaved *2R-48 bp* telomere through
239 its interaction with Ccq1.
240
241 **Removal of the Mre11 nuclease stabilizes the newly formed short telomere in *ccq1*Δ cells.**
242 The two major exonucleases with roles at the telomere and DSBs are exonuclease I (Exo1) and
243 Mre11 of the Mre11-Rad50-Nbs1/Xrs2 (MRN/X) complex [44,48–53]. We tested whether loss of
244 Exo1 or Mre11 slow or relieve the degradation the cleaved *2R-48 bp* proto-telomere in wild type
245 and *ccq1*Δ cells.

246

247 The removal of Exo1 from wild type cells had little effect on *2R-48 bp* proto-telomere cleavage,
248 telomere stability and elongation (Fig. 8A). *2R-0 bp* proto-telomere cleavage was delayed in
249 *exo1*Δ cells without any large increase in stability of this DSB or change in growth (Figs. 8B,D,E,
250 S10A). The cleaved *2R-48 bp* proto-telomere was still rapidly degraded in *ccq1*Δ *exo1*Δ cells,
251 and the growth kinetics were the same as *ccq1*Δ cells (Figs. 8C,E, S10B), although slightly
252 higher levels of the *ura4*$^+$ telomere were detectable at 4 and 6 h in *ccq1*Δ *exo1*Δ cells compared
253 to *ccq1*Δ cells (Figs. 8C, S10B vs. Figs. 4C, S5A). Therefore, Exo1 only makes small
254 contributions to the degradation of the cleaved *2R-48 bp* telomere in *ccq1*Δ cells.

255

256 Removal of Mre11 had much larger effects. Cleavage of the *2R-48 bp* and *2R-0 bp* proto-
257 telomeres occurred similarly in *mre11*Δ and wild type *mre11*$^+$ cells (Figs. 2B-D, 9A,B, S10G). A
258 shorter terminal tract was observed in the *mre11*Δ mutant at 32 h. As *mre11*Δ cells have a
259 longer generation time after induction, the reduced telomere length may be related to the fewer
260 doublings that these cells undergo by 32 h, or another Mre11-related function (Fig. 9I)[43,54].
261 The cleaved *2R-0 bp* proto-telomere fragments were partially stabilized but undetectable after
262 the 8 h time point (Figs. 9B, S10C vs. 2C).

263

264 The *ccq1*Δ *mre11*Δ cells gave a surprising result: the cleaved *2R-48 bp* proto-telomere was
265 much more stable, and the formed *ura4*$^+$ telomere began to shorten at 24 h and was
266 undetectable at 32 h (Figs. 9C,G, S10D). The formed telomere in *ccq1*Δ *mre11*Δ cells was as
267 stable as the telomere formed in *ccq1-T93A* cells that cannot efficiently recruit telomerase (Figs.
268 6B, S8C). Therefore, the rapid degradation of the telomere-repeat capped end in *ccq1*Δ cells
269 requires Mre11, and the absence of Ccq1 reduces telomerase recruitment and elongation of the
270 *ura4*$^+$ telomere.

271

272 To distinguish whether Mre11 protein or its nuclease activity accounts for rapid proto-telomere
273 degradation in *ccq1*Δ cells, similar experiments were performed in *mre11-H134S* strains that
274 lack Mre11 nuclease activity [50]. The *mre11-H134S* wild type and *ccq1*Δ strains gave nearly
275 identical results as the *mre11*Δ strains in proto-telomere cleavage, telomere stability, *2R-0 bp*
276 DSB stability and cell growth, although elongation of the *ura4*$^{+}$ telomere was heterogeneous and
277 reduced compared to *mre11*Δ cells (Fig. 9A-H). While the *ura4*$^{+}$ telomere showed slightly
278 stronger hybridization in *ccq1*Δ *mre11-H134S* cells at 24 and 32 h compared to *ccq1*Δ *mre11*Δ
279 (compare Figs. 9C,G, S10D vs. Figs. 9F,H, S10E), the similar growth rates of *ccq1*Δ *mre11-*
280 *H134S* vs. *ccq1*Δ *mre11*Δ cells (Fig. 9I) suggest that these two cell types were still have the
281 same defects that prevent normal growth. The sum of these data shows that the conversion of
282 the cleaved *2R-48 bp* proto-telomere to a DSB in *ccq1*Δ cells was abrogated by loss of Mre11
283 nuclease activity, and the degradation of the DSB was slowed by the loss of Exo1. Mre11
284 interacts with *S. pombe* telomeres [44] and was detectable at chromosomal ends in *ccq1*Δ cells
285 by ChIP (Fig. S11), showing that Mre11 recruitment to telomeres is Ccq1-independent.
286 Therefore, a novel role of Ccq1 is to restrain the degradation of the newly formed short
287 telomere-repeat capped end by Mre11 nuclease.

288 ## Discussion

289 Requirement for different telomere associated proteins were tested for a role in distinguishing a
290 telomere repeat-capped chromosome end from a DSB using our recently developed *S.* pombe
291 inducible telomere formation system [30]. The 48 bp telomere tract in this system focuses the
292 analysis on the role of the repeats in end protection in the absence of subtelomeres or longer
293 repeat tracts, and allowed testing of viable mutants of telomere-associated proteins on
294 chromosome end protection. Cells lacking Taz1, Rap1 or Poz1 rapidly elongated the short 48
295 bp tract to the extended chromosomal telomere lengths found in these mutants (Figs. 3, S3). In
296 contrast, *rif1*Δ cells initially elongated the terminal tract to wild type lengths and then slowly
297 elongated the telomere repeats to mutant lengths over many generations (Figs. 3, S4). Cells
298 lacking Ccq1 gave the most surprising result: the cleaved proto-telomere was immediately
299 degraded in the same manner as an induced double-strand break (Figs. 4C, S5). These results
300 were unexpected as the previously known telomeric functions of Ccq1 were to recruit
301 telomerase. Chromosomal telomeres with wild type length tracts introduced into *ccq1*Δ cells or
302 *ccq1-T93A* cells gradually shortened over ~80 generations until the terminal repeats tract
303 become extremely short and DNA damage checkpoints were activated [18,23,25,26,28,55]. At
304 this point, *ccq1*Δ cells arrest and/or repair the defective telomere ends by circularizing the
305 chromosome or elongating telomere repeats by a telomerase-independent mechanism [18,26].
306 The immediate degradation of the cleaved proto-telomere in *ccq1*Δ cells was not due to a lack
307 of telomerase activity, as cells lacking telomerase subunits (*est1*Δ and *TER1*Δ) or cells that fail
308 to activate bound telomerase (*tpz1-K75A*)[23,45] maintained the 48 bp tract for more than one
309 day (Figs. 4A,B, 6C, S8E). The rapid degradation of the cut proto-telomere in *ccq1*Δ cells could
310 be blocked by eliminating the DSB processing nuclease activity of Mre11 (Figs. 9, S10D,E).
311 These results, therefore, indicate a novel role for Ccq1 in restraining Mre11-nuclease activity
312 from degrading short tracts of telomere repeats.

313

314 Ccq1 was most likely required to be present at the cleaved short proto-telomere to accomplish
315 this protective function: the *ccq1*Δ strain lacking Ccq1 and the *tpz1-L449A* strain expressing a
316 mutant Tpz1 protein that is defective for Ccq1 interaction showed a similar degradation of the
317 cleaved 48 bp proto-telomere (Figs. 4C, 7B, S5, S9). The requirement for Ccq1 did not appear
318 to be to recruit known Ccq1 associated factors as eliminating these factors did not recapitulate
319 the *ccq1*Δ rapid degradation phenotype. Ccq1 is a component of the histone deacetylase
320 complex SHREC [29]; however, cells lacking the Clr3 catalytic subunit of this complex did not
321 rapidly degrade the cut 48 bp proto-telomere (Fig. 7A). This result is consistent with our
322 previous observations where proto-telomere cleavage allowed the immediate manifestation of
323 the end protective functions that distinguish telomeres from DSBs, but the spreading of
324 telomeric heterochromatin required many generations of growth [30]. Eliminating telomerase
325 activity by removing telomerase RNA (*TER1*Δ) or a telomerase subunit (*est1*Δ) allowed cells to
326 maintain the 48 bp telomere repeat tract for more than one day after cleavage (Fig. 4A,B). In
327 contrast, the *ccq1-T93A* cells (deficient in telomerase recruitment) showed a loss of telomeric
328 *ura4*$^{+}$ hybridization at 24 and 32 h post-cleavage (Fig. 4A,B vs. Figs. 6B, S8C), perhaps
329 reflecting an additional deficiency of Ccq1-T93A at telomeres in these cells. While these
330 differences between telomerase and *ccq1-T93A* mutants may highlight new dynamics as
331 telomeres shorten and lose their function, these affects are greatly delayed compared to the
332 immediate end protection afforded by the 48 bp repeat tract (i.e. suppression of Chk1
333 phosphorylation and the delay in cell division during the first 8 h post cleavage [30](Figs. 2E,
334 4D). Therefore, the end protection properties of the cleaved *2R-48 bp* telomere are most likely
335 due to Ccq1 itself, or an unidentified Ccq1-interacting factor.

336

337 The loss of end protection for the cleaved *2R-48 bp* proto-telomere in *ccq1*Δ cells was partially
338 rescued by loss of Mre11 nuclease activity. Mre11 is part of the MRN complex (MRX in

339 *Saccharomyces cerevisiae*) composed of Mre11, Rad50, and Nbs1 or Xrx2 that initiates the
340 processing of DSBs. It was recently reported that *S. cerevisiae* MRX can be inhibited by the
341 telomere-associated protein Rif2 [56–58]. Rif2p inhibits MRX through an inhibitory motif called
342 MIN, which interacts with the MRX complex through the Rad50 protein [56,57]. While Rif2 is
343 only found in some budding yeasts, the MIN motif was identified in the DNA replication protein
344 Orc4 in some budding yeasts that lack Rif2. Mutation of the MIN motif in Rif2 or Orc4 in
345 different yeasts showed that this motif regulated the steady-state length of the terminal telomeric
346 tracts [56], strongly suggesting an interaction with MRN/X at the telomere. In the *S. pombe*
347 shelterin proteins, a MIN motif was only identified in Taz1, which mediated an interaction
348 between Taz1 and *S. pombe* Rad50 in two-hybrid analyses [56], consistent with the presence of
349 Mre11 with telomeres by ChIP [63](Fig. S11). Mutating the Taz1 MIN motif did not alter the
350 length or the protection of the terminal telomeric tract [56], and the cleaved proto-telomere in
351 *taz1*Δ cells was stable and elongated (Figs. 3A, S2A). Therefore, the role of the Taz1 MIN motif
352 in restraining the Mre11 nuclease activity at the short proto-telomere is not a strong as that of
353 Ccq1.
354
355 Our working model for the restraint of the Mre11 nuclease activity in *S. pombe* is that wild type
356 cells have long enough telomere tracts to recruit sufficient Taz1 and Ccq1 to block MRN-
357 mediate degradation (Fig. 10). Both Taz1 and Ccq1 may protect telomere repeats after
358 replication when the telomeric chromatin is being reassembled or if the replication fork breaks in
359 telomere repeats [6,59]. At telomeres with short repeat tracts, protection may rely on Ccq1 as
360 the amount of Taz1 is limiting (similar to the cleaved *2R-48 bp* proto-telomere). In cells lacking
361 Ccq1, shortening telomeres will be bound by less Taz1 until MRN-mediated degradation is no
362 longer restrained and telomeres are degraded. Telomere repeat tracts would therefore be
363 protected from MRN by the combinatorial actions of Taz1 and Ccq1 under different conditions.
364

365 The Ccq1 and Rif2 proteins that restrain MRN activity at telomeres are limited to relatively
366 closely related fungi [56,60]. *S. pombe* and *S. cerevisiae* are separated by almost one billion
367 years of evolution [61], leading to multiple differences in biological properties that include very
368 different shelterin proteins [1,62]. Nevertheless, both yeasts have evolved specific proteins to
369 reduce Mre11-mediated degradation of the telomere end. This convergent evolution of function
370 raises the possibility that blocking MRN/X activity by domains on specific shelterin proteins is
371 conserved beyond fungi, and potentially in humans, as means for the cell to distinguish
372 telomeres from DSBs.

373 # Materials and Methods

374 **Strains and Media**

375 All *S. pombe* strains used in this study are shown in Tables 4 and S1. Selection for strains
376 containing telomere cassettes was performed in Edinburgh Minimal Media with 3.6 g/l (19 mM)
377 sodium glutamate monohydrate (EMMG) substituted for ammonium chloride without uracil and
378 with appropriate amino acid supplements and 100 µg/ml Hygromycin B Gold (InvivoGen) as
379 described in [63]. Non-selective growth of strains bearing the telomere cassettes was done in
380 EMMG with adenine, histidine, uracil, leucine, lysine, and arginine (EMMG + AHRULK) and
381 without hygromycin (Hyg). Preparation of 10 mM anhydrotetracycline (ahTET) stock and plates
382 was performed as in [64].

383

384 **Cells Transformation and Strain Construction**

385 Cells were grown in EMMG media with appropriate amino acid supplements to OD_{600nm} of 0.5 (1-
386 2 x 10^8 cells) and harvested by centrifugation (3500 g, 5 min, 4°C). The pelleted cells were
387 washed three times with ice-cold 1M Sorbitol (25, 10, and 5 ml). The cells were then resuspended
388 in 0.5 mL ice-cold 1M Sorbitol and mixed with 500 ng of linear DNA (or 50 ng of circular DNA) in
389 a 0.2-cm electroporation cuvette (Bio-Rad). Electroporation was made using the Bio-Rad Gene
390 Pulser, which applied an electric pulse of 11.0 kV/cm for 5 ms. The electroporated cells were
391 then spread onto YES plates and incubated at 32°C overnight. The resulting lawn of cells was
392 then replica plated onto the appropriate selective media and incubated at 32°C until colonies
393 formed (adapted from [65]).

394

395 Gene deletion or mutations were made with a kanMX6 or natMX4 PCR fragment amplified by
396 PCR with at least 250 bp of homology on the 5' and 3' of the targeted gene. The ccq1 deletion

397 was always the last deletion made in all the strains listed in Table S4 to minimize the number of
398 generations before the telomere formation induction (less than 50 generations).
399
400 **Induction of *I-SceI***
401 Cells containing the telomere cassettes were grown under selection overnight (EMMG + AHR +
402 Hyg) and diluted in non-selective media (EMMG + AHRULK) for exponential growth for 3-4 h.
403 Untreated cells (3-5 x 10^8) were removed, pelleted, and washed in sterile, milli-Q purified water
404 before freezing the cell pellets at -80°C. The remaining cells were treated with ahTET, added to
405 a final concentration of 9 µM. Cells were then collected at various time points, pelleted,
406 washed, and frozen as above.
407
408 **Southern Blot Analysis**
409 Cells (3-5 x10^8) were collected at each time point and used to prepare genomic DNA as in [66].
410 Genomic DNA (50 µg) was digested with 20 units of *Sca* I-HF (NEB) overnight at 37°C. The
411 digested DNA was resolved on a 1.2% agarose gel (6 h at 100 V) and transferred onto a
412 Hybond N+ positively charged nylon membrane (Amersham - GE healthcare). The membrane
413 then was crosslinked with UV and hybridized (60°C, overnight) by labeled probes produced by
414 PCR with u4ScaProbe_S + u4ScaProbe_AS (*ura4*$^+$ probe), SV40ScaProbe_S +
415 SV40ScaProbe_AS (*hph*$^+$ probe), or abo1-probe_S + abo1-probe_AS (*abo1*$^+$ probe as a loading
416 control) using 100 µCi of [α-32P-dCTP] (6000 Ci/mmol, PerkinElmer) as previously described in
417 [30] (primer sequences are shown in Tables 5). The labeled and washed membrane was
418 exposed 1-2 days into a cassette containing a phosphor screen. The radiolabeled DNA
419 quantification acquisition was made using the Amersham Typhoon IP Biomolecular Imager. All
420 the quantifications and telomere band size measurements were then made using Image
421 Quant™ TL 8.2 Software for Windows.
422

423 **Quantitative Survivor Plating Assay**

424 Cells were plated onto non-selective EMMG with or without ahTET at ~200 cells per plate and
425 grown for 3-4 days at 32°C. The colonies were then counted, and the survival percentage was
426 calculated by the number of individual colonies formed on ahTET plates (induced condition)
427 over to the number of colonies formed on plates without ahTET (uninduced condition). A
428 minimum of 300 colonies were counted for each strain for each assay.

429

430 **Doubling time calculation**

431 To measure the OD_{600nm}, a WPA CO 8000 Cell Density Meter was used, and cultures were
432 diluted to obtain a reading between 0.3 and 1.2, corresponding to the linear range between OD
433 measurement and cell concentration. OD_{600nm} was measured before the induction, at 4, 8, 12 or
434 16, 24 and/or 32 h, and were combined in three categories: uninduced, 0-8 h pos-induction, and
435 8-24 or 8-32 h post-induction. The doubling time calculation was made using the formula:

436 $$doubling\ time\ = \frac{\ln(2)}{gr}$$ where gr is the growth rate and $$gr = \frac{\ln\left(\frac{OD_{tx}}{OD_{t0}}\right)}{t}$$

437

438 **Statistical comparisons**

439 Doubling time comparisons used the uninduced condition of each strain tested as the standard.
440 Wild type *2R-48 bp* strain was used as the standard for telomere length comparison after I-SceI
441 cleavage. For ChIP: *2R-0 bp* or wild type *2R-48 bp* untagged strains values were used as the
442 standard. Comparisons for survival used wild type strains as the standard. The t-tests were
443 performed with Microsoft Excel for Mac (v.16.52).

444

445 **ChIP Assay**

446 At each time point, 2-3 $x10^9$ cells in 200 ml final were processed as previously described in [30]
447 with minor modifications. Cells were cross-linked with 1% formaldehyde and washed twice with

448 cold TBS buffer (50 mM Tris-HCl pH 7.5, 150 mM NaCl) supplemented with 125mM final of
449 Glycine. Cell pellets were resuspended in ChIP-lysis buffer and lysed using the Precellys
450 homogenizer (Bertin Instruments) for a mechanical disruption with 0.5 mm glass beads (Biospec
451 11079105) using 3 cycles of 30 sec followed by 2 min on ice. The lysate was sonicated for 10
452 cycles on maximum power (30 sec ON and 59 sec OFF) in a Diagenode Bioruptor XL with
453 sample tubes soaked in an ice water bath. Solubilized chromatin protein concentration was
454 measured using the Bio-Rad protein assay, and all the samples were standardized to the same
455 concentration in 800 µl ChIP-lysis buffer. 790 µl was used for each ChIP sample, while 10 µl
456 was saved as input. Mouse monoclonal antibodies: M2 anti-FLAG (F3165, Sigma-Aldrich), anti-
457 myc tag antibody (9E10, Abcam ab32) or anti-GFP (632375, Clontech) were added to the lysate
458 and incubated while rocking for 3 h at 4°C. 50 µl of Dynabeads™ Protein G (Invitrogen) was
459 then added for rocking 3 additional hours at 4°C. Beads were washed and resuspended in 110
460 µl of TES (1 x TE with 1% SDS). The supernatant (100 µl) was recovered and separated from
461 the beads to be incubated in at 65°C, 8 h in a PCR block, to reverse cross-linking. For input
462 samples, TES buffer (90 µl) was added and the tubes were incubated with the ChIP samples.
463 Then, all the samples were treated with RNase A 30 min at 37°C and Proteinase K for 30
464 additional minutes at 37°C and purified by QIAgen PCR purification column. All the time points
465 from the same figure were processed for ChIP assay at the same time, and 3 independent
466 biological replications were made. For the qPCR analysis, input samples were diluted to 1/10
467 with ddH_2O, while ChIP samples were not diluted. Template DNA (2 µl) was added to 5 µl of
468 Roche LightCycler 480 SYBR Green I Master (2X), and primers were added to a final
469 concentration of 0.6 µM for a 10 µl total reaction volume. Each sample was run at least twice
470 on the same 384-well PCR plate (Roche LightCycler 480 Multiwell Plate 384, clear) in a Roche
471 LightCycler 480. The ChIP and input signals were calculated using standard dilution series.
472 The ratios ChIP/input signal are presented.

Acknowledgments

We thank Carly Kerr for technical assistance and members of the Runge lab for helpful discussions during the course of this work, and Stéphane Coulon and Bibo Li for comments of the manuscript. We thank Katsunori Tomita, Toru Nakamura, Peter Baumann, Feng Qiao, Tony Carr and Paul Russell for *S. pombe* bearing mutations used to construct our strains. This work and JA were supported for by NSF grant 1908875 to KWR. KWR was supported by this NSF grant, NIH grant R01AG051601 and the Lerner Research Institute.

Author Contributions

Conceptualization, methodology and writing: JA and KWR. Investigation and visualization: JA. Funding Acquisition: KWR.

References

1. Wellinger RJ, Zakian VA. Everything you ever wanted to know about *Saccharomyces cerevisiae* telomeres: beginning to end. Genetics. 2012 Aug;191(4):1073–105.
2. Pfeiffer V, Lingner J. Replication of telomeres and the regulation of telomerase. Cold Spring Harb Perspect Biol. 2013 May 1;5(5):a010405.
3. de Lange T. Shelterin-Mediated Telomere Protection. Annu Rev Genet. 2018 Nov 23;52:223–47.
4. Moser BA, Subramanian L, Khair L, Chang Y-T, Nakamura TM. Fission yeast Tel1(ATM) and Rad3(ATR) promote telomere protection and telomerase recruitment. PLoS Genet. 2009 Aug 28;5(8):e1000622.
5. Xue J, Chen H, Wu J, Takeuchi M, Inoue H, Liu Y, et al. Structure of the fission yeast *S. pombe* telomeric Tpz1-Poz1-Rap1 complex. Cell Res. 2017 Dec 21;27(12):1503–20.
6. Bonnell E, Pasquier E, Wellinger RJ. Telomere Replication: Solving Multiple End

498 Replication Problems. Front Cell Dev Biol. 2021 Apr 1;9.
499 7. Gottschling DE, Aparicio OM, Billington BL, Zakian VA. Position effect at *S. cerevisiae*
500 telomeres: reversible repression of Pol II transcription. Cell. 1990 Nov 16;63(4):751–62.
501 8. Wilkie AOM, Lamb J, Harris PC, Finney RD, Higgs DR. A truncated human chromosome
502 16 associated with alpha thalassaemia is stabilized by addition of telomeric repeat
503 (TTAGGG)n. Nature. 1990 Aug 30;346(6287):868–71.
504 9. Nimmo ERR, Cranston G, Allshire RCC. Telomere-associated chromosome breakage in
505 fission yeast results in variegated expression of adjacent genes. EMBO J. 1994 Aug
506 15;13(16):3801–11.
507 10. Kanoh J, Ishikawa F. spRap1 and spRif1, recruited to telomeres by Taz1, are essential
508 for telomere function in fission yeast. Curr Biol. 2001 Oct;11(20):1624–30.
509 11. Hayano M, Kanoh Y, Matsumoto S, Renard-Guillet C, Shirahige K, Masai H. Rif1 is a
510 global regulator of timing of replication origin firing in fission yeast. Genes Dev. 2012 Jan
511 15;26(2):137–50.
512 12. Mattarocci S, Reinert JK, Bunker RD, Fontana GA, Shi T, Klein D, et al. Rif1 maintains
513 telomeres and mediates DNA repair by encasing DNA ends. Nat Struct Mol Biol. 2017
514 Jul;24(7):588–95.
515 13. Shubin CB, Greider CW. The role of Rif1 in telomere length regulation is separable from
516 its role in origin firing. Elife. 2020 Jun 29;9.
517 14. Mirman Z, Lottersberger F, Takai H, Kibe T, Gong Y, Takai K, et al. 53BP1-RIF1-shieldin
518 counteracts DSB resection through CST- and Polα-dependent fill-in. Nature.
519 2018;560(7716):112–6.
520 15. Noordermeer SM, Adam S, Setiaputra D, Barazas M, Pettitt SJ, Ling AK, et al. The
521 shieldin complex mediates 53BP1-dependent DNA repair. Nature. 2018;560(7716):117–
522 21.
523 16. Cooper JP, Nimmo ER, Allshire RC, Cech TR. Regulation of telomere length and function

524 by a Myb-domain protein in fission yeast. Nature. 1997;385(6618 LB-702):744–7.
525 17. Chikashige Y, Hiraoka Y. Telomere binding of the Rap1 protein is required for meiosis in
526 fission yeast. Curr Biol. 2001 Oct;11(20):1618–23.
527 18. Miyoshi T, Kanoh J, Saito M, Ishikawa F. Fission yeast Pot1-Tpp1 protects telomeres and
528 regulates telomere length. Science. 2008 Jun 6;320(5881):1341–4.
529 19. Baumann P. Pot1, the Putative Telomere End-Binding Protein in Fission Yeast and
530 Humans. Science. 2001 May 11;292(5519):1171–5.
531 20. Jun H-I, Liu J, Jeong H, Kim J-K, Qiao F. Tpz1 controls a telomerase-nonextendible
532 telomeric state and coordinates switching to an extendible state via Ccq1. Genes Dev.
533 2013 Sep 1;27(17):1917–31.
534 21. Pan L, Hildebrand K, Stutz C, Thomä N, Baumann P. Minishelterins separate telomere
535 length regulation and end protection in fission yeast. Genes Dev. 2015 Jun
536 1;29(11):1164–74.
537 22. Liu J, Hu X, Bao K, Kim J-K, Zhang C, Jia S, et al. The cooperative assembly of shelterin
538 bridge provides a kinetic gateway that controls telomere length homeostasis. Nucleic
539 Acids Res. 2021 Aug 20;49(14):8110–9.
540 23. Moser BA, Chang Y-T, Kosti J, Nakamura TM. Tel1ATM and Rad3ATR kinases promote
541 Ccq1-Est1 interaction to maintain telomeres in fission yeast. Nat Struct Mol Biol. 2011
542 Nov 20;18(12):1408–13.
543 24. Webb CJ, Zakian VA. *Schizosaccharomyces pombe* Ccq1 and TER1 bind the 14-3-3-like
544 domain of Est1, which promotes and stabilizes telomerase-telomere association. Genes
545 Dev. 2012 Jan 1;26(1):82–91.
546 25. Yamazaki H, Tarumoto Y, Ishikawa F. Tel1(ATM) and Rad3(ATR) phosphorylate the
547 telomere protein Ccq1 to recruit telomerase and elongate telomeres in fission yeast.
548 Genes Dev. 2012 Feb 1;26(3):241–6.
549 26. Tomita K, Cooper JP. Fission yeast Ccq1 is telomerase recruiter and local checkpoint

550 controller. Genes Dev. 2008 Dec 15;22(24):3461–74.
551 27. Harland JL, Chang Y-T, Moser BA, Nakamura TM. Tpz1-Ccq1 and Tpz1-Poz1
552 interactions within fission yeast shelterin modulate Ccq1 Thr93 phosphorylation and
553 telomerase recruitment. PLoS Genet. 2014 Oct 16;10(10):e1004708.
554 28. Moser BA, Raguimova ON, Nakamura TM. Ccq1-Tpz1TPP1 interaction facilitates
555 telomerase and SHREC association with telomeres in fission yeast. Mol Biol Cell. 2015
556 Nov 1;26(21):3857–66.
557 29. Sugiyama T, Cam HP, Sugiyama R, Noma K, Zofall M, Kobayashi R, et al. SHREC, an
558 effector complex for heterochromatic transcriptional silencing. Cell. 2007 Feb
559 9;128(3):491–504.
560 30. Wang J*, Eisenstatt JR*, Audry J*, Cornelius K, Shaughnessy M, Berkner KL, et al. A
561 Heterochromatin Domain Forms Gradually at a New Telomere and Is Dynamic at Stable
562 Telomeres. Mol Cell Biol. 2018 May 1;38(15). (*co-first authors)
563 31. al-Khodairy F, Carr AM. DNA repair mutants defining G2 checkpoint pathways in
564 *Schizosaccharomyces pombe*. EMBO J. 1992 Apr;11(4):1343–50.
565 32. Xue Y, Marvin ME, Ivanova IG, Lydall D, Louis EJ, Maringele L. Rif1 and Exo1 regulate
566 the genomic instability following telomere losses. Aging Cell. 2016;15(3):553–62.
567 33. Fontana GA, Reinert JK, Thomä NH, Rass U. Shepherding DNA ends: Rif1 protects
568 telomeres and chromosome breaks. Microb cell. 2018 May 17;5(7):327–43.
569 34. Wang J, Zhang H, Al Shibar M, Willard B, Ray A, Runge KW. Rif1 phosphorylation site
570 analysis in telomere length regulation and the response to damaged telomeres. DNA
571 Repair (Amst). 2018;65:26–33.
572 35. Nurse P, Thuriaux P, Nasmyth K. Genetic control of the cell division cycle in the fission
573 yeast *Schizosaccharomyces pombe*. Mol Gen Genet MGG. 1976 Jan;146(2):167–78.
574 36. Miyoshi T, Sadaie M, Kanoh J, Ishikawa F. Telomeric DNA ends are essential for the
575 localization of Ku at telomeres in fission yeast. J Biol Chem. 2003 Jan 17;278(3):1924–

576 31.
577 37. Tomita K, Bez C, Fennell A, Cooper JP. A single internal telomere tract ensures meiotic
578 spindle formation. EMBO Rep. 2013 Mar 1;14(3):252–60.
579 38. Audry J, Maestroni L, Delagoutte E, Gauthier T, Nakamura TM, Gachet Y, et al. RPA
580 prevents G-rich structure formation at lagging-strand telomeres to allow maintenance of
581 chromosome ends. EMBO J. 2015 Jul 14;34(14):1942–58.
582 39. Webb CJ, Zakian VA. Telomerase RNA stem terminus element affects template
583 boundary element function, telomere sequence, and shelterin binding. Proc Natl Acad
584 Sci. 2015;112(36):11312–7.
585 40. Naito T, Matsuura A, Ishikawa F. Circular chromosome formation in a fission yeast
586 mutant defective in two ATM homologues. Nat Genet. 1998 Oct;20(2):203–6.
587 41. Bentley NJ, Holtzman DA, Flaggs G, Keegan KS, DeMaggio A, Ford JC, et al. The
588 *Schizosaccharomyces pombe* rad3 checkpoint gene. EMBO J. 1996 Dec 2;15(23):6641–
589 51.
590 42. Nakamura K, Okamoto A, Katou Y, Yadani C, Shitanda T, Kaweeteerawat C, et al.
591 Rad51 suppresses gross chromosomal rearrangement at centromere in
592 *Schizosaccharomyces pombe*. EMBO J. 2008 Nov 19;27(22):3036–46.
593 43. Manolis KG, Nimmo ER, Hartsuiker E, Carr AM, Jeggo PA, Allshire RC. Novel functional
594 requirements for non-homologous DNA end joining in *Schizosaccharomyces pombe.*
595 EMBO J. 2001 Jan 15;20(1–2):210–21.
596 44. Nakamura TM, Moser BA, Russell P. Telomere binding of checkpoint sensor and DNA
597 repair proteins contributes to maintenance of functional fission yeast telomeres. Genetics.
598 2002 Aug;161(4):1437–52.
599 45. Armstrong CA, Pearson SR, Amelina H, Moiseeva V, Tomita K. Telomerase Activation
600 after Recruitment in Fission Yeast. Curr Biol. 2014 Sep;24(17):2006–11.
601 46. Shampay J, Blackburn EH. Generation of telomere-length heterogeneity in

602 *Saccharomyces cerevisiae*. Proc Natl Acad Sci. 1988 Jan 1;85(2):534–8.
603 47. Job G, Brugger C, Xu T, Lowe BR, Pfister Y, Qu C, et al. SHREC Silences
604 Heterochromatin via Distinct Remodeling and Deacetylation Modules. Mol Cell.
605 2016;62(2):207–21.
606 48. Mimitou EP, Symington LS. Sae2, Exo1 and Sgs1 collaborate in DNA double-strand
607 break processing. Nature. 2008 Oct 9;455(7214):770–4.
608 49. Nicolette ML, Lee K, Guo Z, Rani M, Chow JM, Lee SE, et al. Mre11-Rad50-Xrs2 and
609 Sae2 promote 5' strand resection of DNA double-strand breaks. Nat Struct Mol Biol. 2010
610 Dec;17(12):1478–85.
611 50. Williams RS, Moncalian G, Williams JS, Yamada Y, Limbo O, Shin DS, et al. Mre11
612 dimers coordinate DNA end bridging and nuclease processing in double-strand-break
613 repair. Cell. 2008 Oct 3;135(1):97–109.
614 51. Zhu Z, Chung W-H, Shim EY, Lee SE, Ira G. Sgs1 helicase and two nucleases Dna2 and
615 Exo1 resect DNA double-strand break ends. Cell. 2008 Sep 19;134(6):981–94.
616 52. Maringele L, Lydall D. EXO1-dependent single-stranded DNA at telomeres activates
617 subsets of DNA damage and spindle checkpoint pathways in budding yeast yku70Delta
618 mutants. Genes Dev. 2002 Aug 1;16(15):1919–33.
619 53. Kibe T, Tomita K, Matsuura A, Izawa D, Kodaira T, Ushimaru T, et al. Fission yeast
620 Rhp51 is required for the maintenance of telomere structure in the absence of the Ku
621 heterodimer. Nucleic Acids Res. 2003;31(17):5054–63.
622 54. Wilson S, Warr N, Taylor DL, Watts FZ. The role of *Schizosaccharomyces pombe* Rad32,
623 the Mre11 homologue, and other DNA damage response proteins in non-homologous
624 end joining and telomere length maintenance. Nucleic Acids Res. 1999 Jul
625 1;27(13):2655–61.
626 55. Armstrong CA, Moiseeva V, Collopy LC, Pearson SR, Ullah TR, Xi ST, et al. Fission
627 yeast Ccq1 is a modulator of telomerase activity. Nucleic Acids Res. 2018;46(2):704–16.

628 56. Khayat F, Cannavo E, Alshmery M, Foster WR, Chahwan C, Maddalena M, et al.
629 Inhibition of MRN activity by a telomere protein motif. Nat Commun. 2021;12(1):3856.
630 57. Roisné-Hamelin F, Pobiega S, Jézéquel K, Miron S, Dépagne J, Veaute X, et al.
631 Mechanism of MRX inhibition by Rif2 at telomeres. Nat Commun. 2021;12(1):2763.
632 58. Rosas Bringas FR, Stinus S, de Zoeten P, Cohn M, Chang M. Rif2 protects Rap1-
633 depleted telomeres from MRX-mediated degradation in *Saccharomyces cerevisiae*. Elife.
634 2022;11.
635 59. Miller KM, Rog O, Cooper JP. Semi-conservative DNA replication through telomeres
636 requires Taz1. Nature. 2006 Apr 6;440(7085):824–8.
637 60. Rhind N, Chen Z, Yassour M, Thompson DA, Haas BJ, Habib N, et al. Comparative
638 functional genomics of the fission yeasts. Science. 2011;332(6032):930–6.
639 61. Hedges SB. The origin and evolution of model organisms. Nat Rev Genet.
640 2002;3(11):838–49.
641 62. Moser BA, Nakamura TM. Protection and replication of telomeres in fission yeast.
642 Biochem cell Biol. Oct;87(5):747–58.
643 63. Moreno S, Klar A, Nurse P. Molecular genetic analysis of fission yeast
644 *Schizosaccharomyces pombe*. Methods Enzymol. 1991;194:795–823.
645 64. Sunder S, Greeson-Lott NT, Runge KW, Sanders SL. A new method to efficiently induce
646 a site-specific double-strand break in the fission yeast *Schizosaccharomyces pombe*.
647 Yeast. 2012 Jul;29(7):275–91.
648 65. Suga M, Hatakeyama T. High efficiency transformation of *Schizosaccharomyces pombe*
649 pretreated with thiol compounds by electroporation. Yeast. 2001 Aug;18(11):1015–21.
650 66. Ray A, Runge KW. The yeast telomere length counting machinery is sensitive to
651 sequences at the telomere-nontelomere junction. Mol Cell Biol. 1999 Jan;19(1):31–45.
652

653 **Figure Legends**

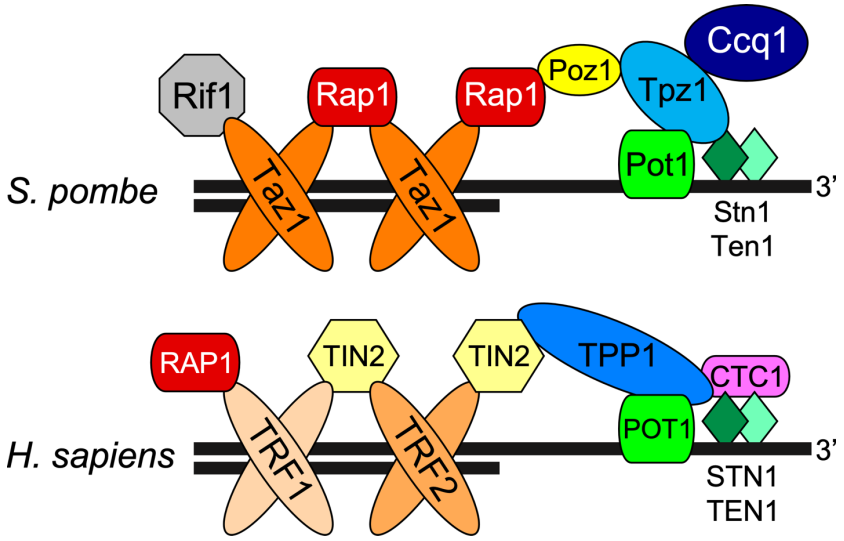

654

655 **Fig. 1. *S. pombe* and *H. sapiens* telomere-capping complexes** share a similar molecular
656 architecture. The human complex (called shelterin) and fission yeast complex are visualized as
657 a conserved bridge structure [22] with a double-stranded telomere DNA protein (TRF1-
658 TRF2/Taz1) connected to the single-stranded telomere DNA protein POT1 by non-DNA-binding
659 proteins (TIN2-TPP1/Rap1-Poz1-Tpz1). Homologous and orthologous proteins are shown in
660 similar colors.

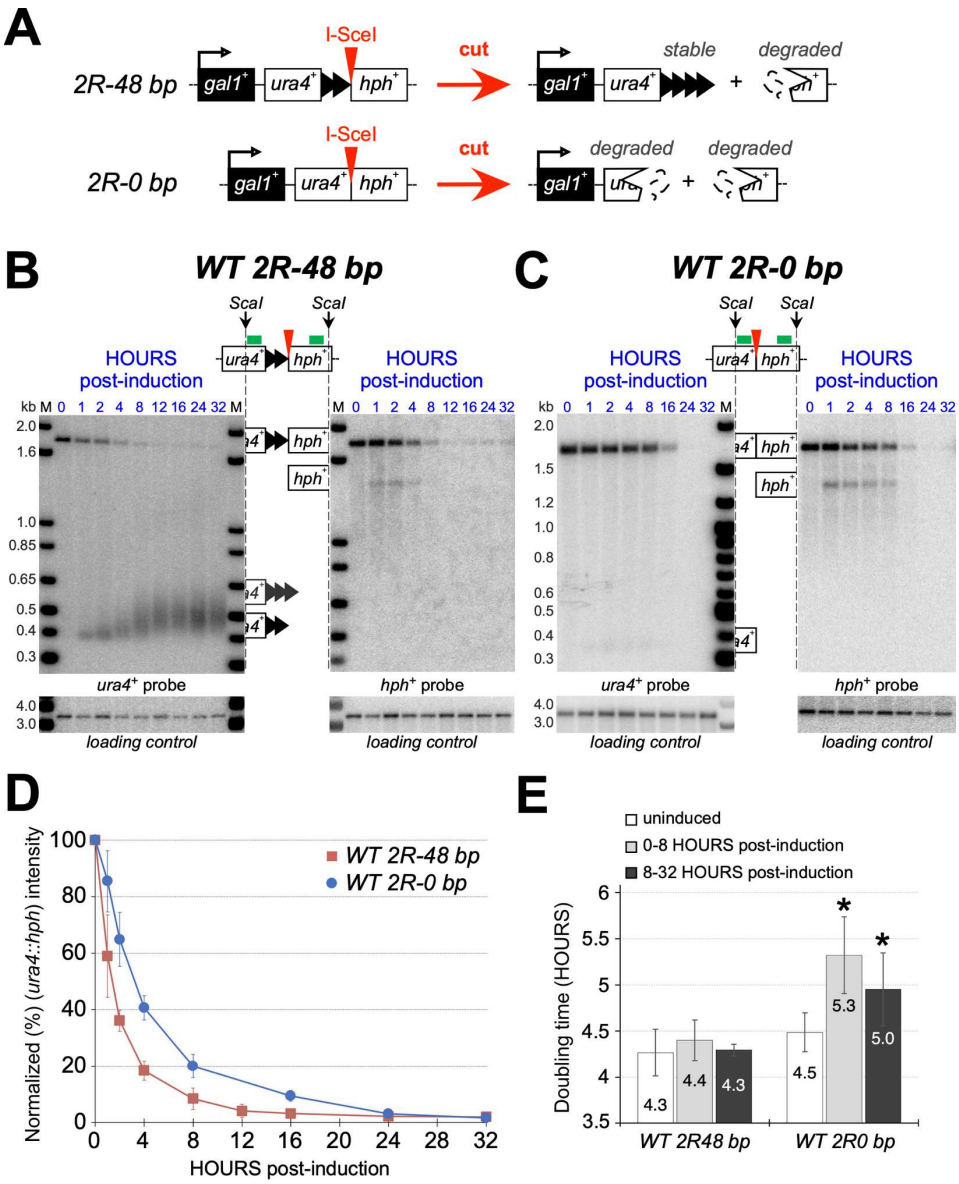

Fig. 2. I-SceI cleavage next to telomere repeats leads to the formation of a new telomere, whereas cleavage in the absence of these repeats produces a rapidly degraded DSB. (A) Schematic of the proto-telomere cassettes at the right end of chromosome 2 and the consequences of I-SceI induction [30](the full system is described in Fig. S1). The I-SceI site is marked by a red triangle. The *2R-48 bp* proto-telomere contains 48 bp of telomere repeats, while *2R-0 bp* has no such repeats. Telomere repeats are indicated by black triangles. Genes are indicated by boxes and degrade DNA by jagged edges and small lines. **(B)** Wild type (WT) *2R-48 bp* exponentially growing cells were treated with ahTET (9 μM final) to induce the I-SceI

670 enzyme expression. Aliquots were taken either prior to induction (0 h) or after induction (1 to 32
671 h). The genomic DNA was then extracted, digested with *Sca* I, and analyzed by Southern
672 analysis using probes *ura4*$^+$, *hph*$^+$ (denoted by green bars above each locus), or *abo1*$^+$ as a
673 loading control. A schematic of the *2R-48 bp* cassette shows the positions of the *Sca* I sites,
674 and the truncated schematics indicate which fragments formed the bands on the Southern blot.
675 The numbers in blue on top of the blots represent the hours post-induction. Molecular weight
676 standards are shown (M). The modal terminal restriction fragment sizes of the *ura4*$^+$ cut band
677 are presented in Table S6. **(C)** Cells bearing the *2R-0 bp* cassette were treated and analyzed
678 as in Fig. 2B. **(D)** Normalized intensities of the 1.8 kb uncut *ura4::hph* bands of the inductions
679 shown in B and C. Normalization is the average of the Typhoon IP biomolecular Imager
680 (Amersham) signals (quantified using Image Quant™ TL 8.2 Software) of the *ura4*$^+$, or *hph*$^+$
681 probe normalized to the loading control (*abo1*$^+$ probe) signal for each lane. The 0 h time point
682 (uninduced condition) is represented as 100% for each strain. Error bars show standard
683 deviations from three independent assays (values are in Table S1). **(E)** Doubling times of the
684 cell cultures were determined by OD_{600nm} prior to the ahTET induction (uninduced), 0-8 h post-
685 induction, and 8-32 h post-induction. Error bars show standard deviations from at least three
686 independent assays. Statistically significant differences ($p<0.05$) are indicated by an asterisk.

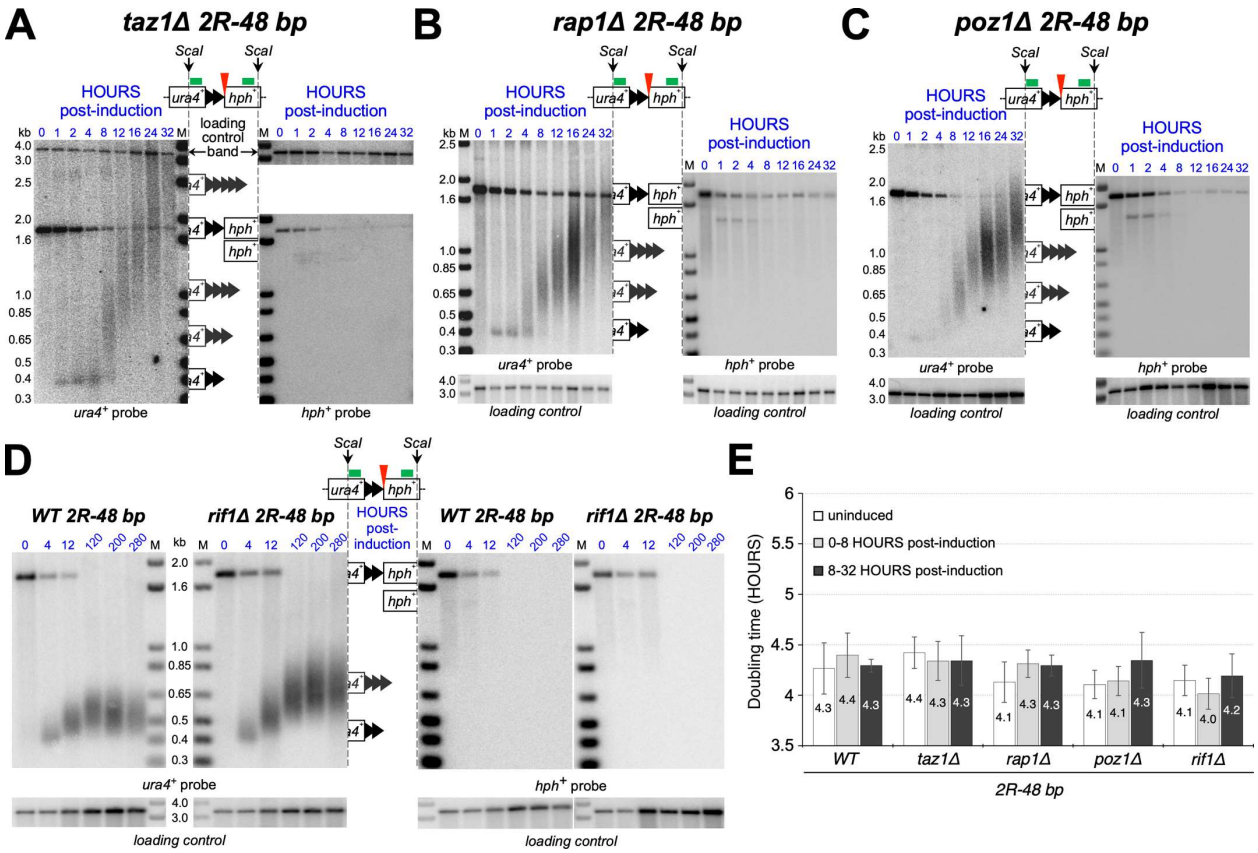

Fig. 3. Cells lacking Taz1, Rap1, Poz1 and Rif1 produce stable telomere repeat-capped ends to reach new equilibrium telomere lengths. *taz1*Δ **(A)**, *rap1*Δ **(B)**, or *poz1*Δ **(C)** cells bearing the *2R-48 bp* proto-telomere were treated with ahTET (9 μM final) and analyzed by Southern blot as in Fig. 2B. The modal terminal restriction fragment sizes of the *ura4*$^+$ cut band are presented in Fig. S3D and Table S6. The *taz1*Δ *ura4*$^+$ probe panel is shown as the full gel to present the long, disperse telomere repeat hybridization. Additional Southern blots from independent experiments are shown in Fig. S3A. The final telomere repeat tract lengths are similar to those described for the original mutants (median lengths of 1.0 to 2.5 kb, ranging from 0.5 to 5 kb [10,16,18]). **(D)** *WT or rif1*Δ cells bearing the *2R-48 bp* proto-telomere were treated with ahTET (9 μM final) to induce the I-SceI enzyme expression. Aliquots were first taken either prior to induction (0 h) and after induction (1 to 12 h). At 12 h, cells were struck for a single colony on rich media (YES) and grown for 3 days at 32°C. Portions of several individual resulting colonies were tested for loss of *hph*$^+$ by failure to grow on plates with 100 μg/ml

701 hygromycin. A hygromycin-sensitive colony was inoculated in non-selective EMMG media with
702 ahTET, and serial dilutions from time points 120, 200, and 280 h were collected and analyzed
703 by Southern blot as in Fig. 2B. An additional Southern blot is shown in Fig. S4B. **(E)** Doubling
704 times of the cell cultures were determined by OD_{600nm} prior to the ahTET induction (uninduced),
705 0-8 h post-induction and 8-32 h post-induction. Error bars show standard deviations from at
706 least three independent assays. The wild type values from Fig. 2E are included for comparison.
707

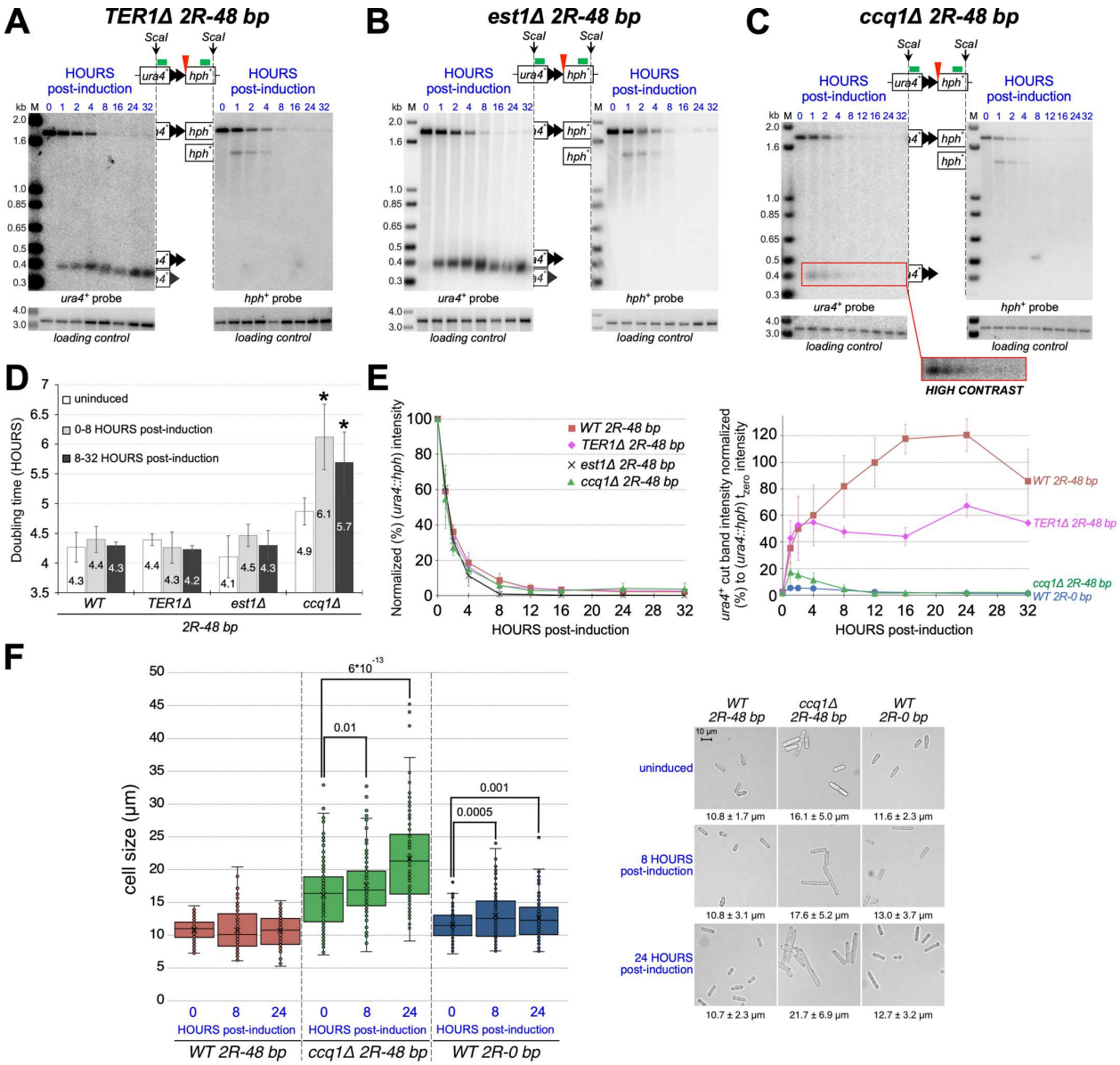

708

709 **Fig. 4. Cells lacking the telomerase components TER1 or Est1 form a short, stable**
710 **telomere while loss of Ccq1 causes rapid degradation similar to a DSB.** Cells lacking
711 telomerase RNA TER1 **(A)**, Est1 **(B)**, or Ccq1 **(C)** and bearing the *2R-48 bp* cassette were
712 treated and analyzed as in Fig. 2B. The modal terminal restriction fragment sizes of the *ura4*$^+$
713 cut band are presented in Table S6. An additional *ccq1*Δ Southern blot is shown in Fig. S5. **(D)**
714 Doubling times of the cell cultures were determined by OD_{600nm} prior to the ahTET induction
715 (uninduced), 0-8 h post-induction, and 8-32 h post-induction. Error bars show standard
716 deviations from at least three independent assays. Statistically significant differences (p<0.05)
717 are indicated by an asterisk. The wild type values from Fig. 2E are included for comparison.
718 **(E) Left panel.** Intensities normalized to the loading control of the 1.8 kb uncut *ura4::hph* bands
719 of the inductions shown in Figs. 2B and 4A-C, derived as in Fig. 2D. The wild type *2R-48 bp*
720 values from Fig. 2D are included for comparison. **Right panel.** Normalized intensities of the
721 *ura4*$^+$ cut bands of the inductions shown in Figs. 2B,C and 4A,C. The *est1*Δ cell values are not
722 plotted as they are nearly identical to those of *TER1*Δ cells (Table S6). Normalization is the
723 average of the Typhoon IP biomolecular Imager (Amersham) signals (quantified using Image
724 Quant™ TL 8.2 Software) of the *ura4*$^+$ bands (using the *ura4*$^+$ probe) divided by the 1.8 kb
725 *ura4::hph* band intensity before induction (0 h)(using the *ura4*$^+$ probe, in the same membrane)
726 for each lane. The error bars for *TER1*Δ *2R-48 bp* and *ccq1*Δ *2R-48 bp* strains are derived from
727 three independent Southern blots, and the *est1*Δ *2R-48 bp* strain error bars are from two
728 independent Southern blots (values are in Tables S1 and S3). **(F) Left panel:** Cell lengths (n >
729 110 of each strain) prior to the ahTET induction (0 h) and 8 and 24 h post-induction are
730 represented. Statistically significant values (p<0.05, t-test) are indicated by the black numbers
731 in the graph. **Right panel:** Cells observations (Brightfield mode) made by using a DM4B
732 microscope (Leica) with the DFC7000T Digital Camera (Leica) and processed using the Leica
733 Application Suite X v3.7.2.22383 (for Windows). The numbers below indicate the average cell
734 length ± standard deviation in each condition (in micrometers). Cell measurements were made

735 using the ruler tool of the Adobe Photoshop 2021 software (v22.5.4 for Mac) and normalized to

736 the scale bar (10 um) generated into the image by the Leica Application Suite X.

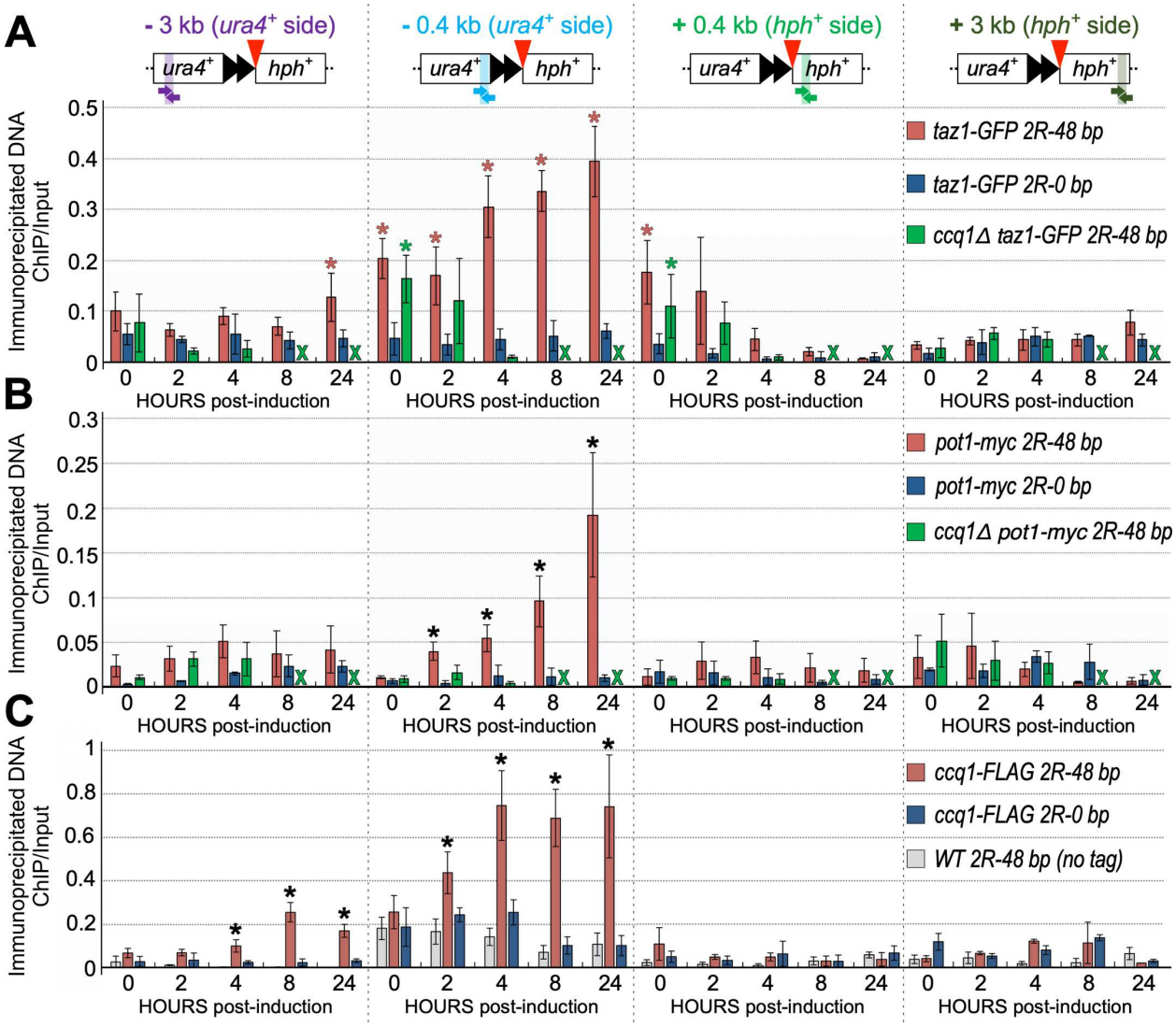

737

738 **Fig. 5. ChIP analyses of Taz1, Ccq1, and Pot1 at the proto-telomere before and after**

739 **cleavage in wild type and *ccq1*Δ cells.** ChIP of *taz1-GFP* **(A)**, *pot1-myc* **(B)**, *or Ccq1-FLAG*

740 **(C)** cells bearing the *2R-0 bp* or the *2R-48 bp* cassettes in a wild type and *ccq1*Δ background.

741 Representative Southern blots, cut efficiency quantifications and doubling times of these strains

742 are shown in Fig. S6. The ChIP immunoprecipitations used an anti-GFP antibody (**A**, 632375,

743 Clontech), an anti-myc antibody (**B**, 9E10, Abcam ab32), or an anti-FLAG M2 antibody (**C**,

744 F3165, Sigma-Aldrich). The immunoprecipitated DNA was analyzed by qPCRs using 4 pairs of
745 primers (Table S5) as represented by the arrows in the telomere cassette schematics above the
746 graphs. "-3 kb" (in purple) and "-0.4 kb" (in blue) are in the *ura4*$^+$ gene that forms the telomere,
747 and "+0.4 kb" (in green) and "+3 kb" (in dark green) are located in the *hph*$^+$ gene that is
748 degraded. For the *ccq1*Δ *taz1-GFP* and *ccq1*Δ *pot1-myc 2R-48 bp* strains, only the 0, 2, and 4
749 h time points aliquots were taken as almost all the *ura4*$^+$ DNA cut fragment is degraded,
750 preventing accurate quantitation. "X" means not measured. Cutting efficiencies of the tagged
751 (Fig. S6) and untagged (Figs. 2D and 4E) strains were similar. Error bars show standard
752 deviations from three independent assays. Statistically significant differences (p<0.05) are
753 indicated by an asterisk. In (**A**), a red asterisk means a statistically significant difference
754 between *taz1-GFP 2R48 bp* and *taz1-GFP 2R0 bp*, whereas a green asterisk is between *ccq1*Δ
755 *taz1-GFP 2R48 bp* and *taz1-GFP 2R0 bp* strains.
756

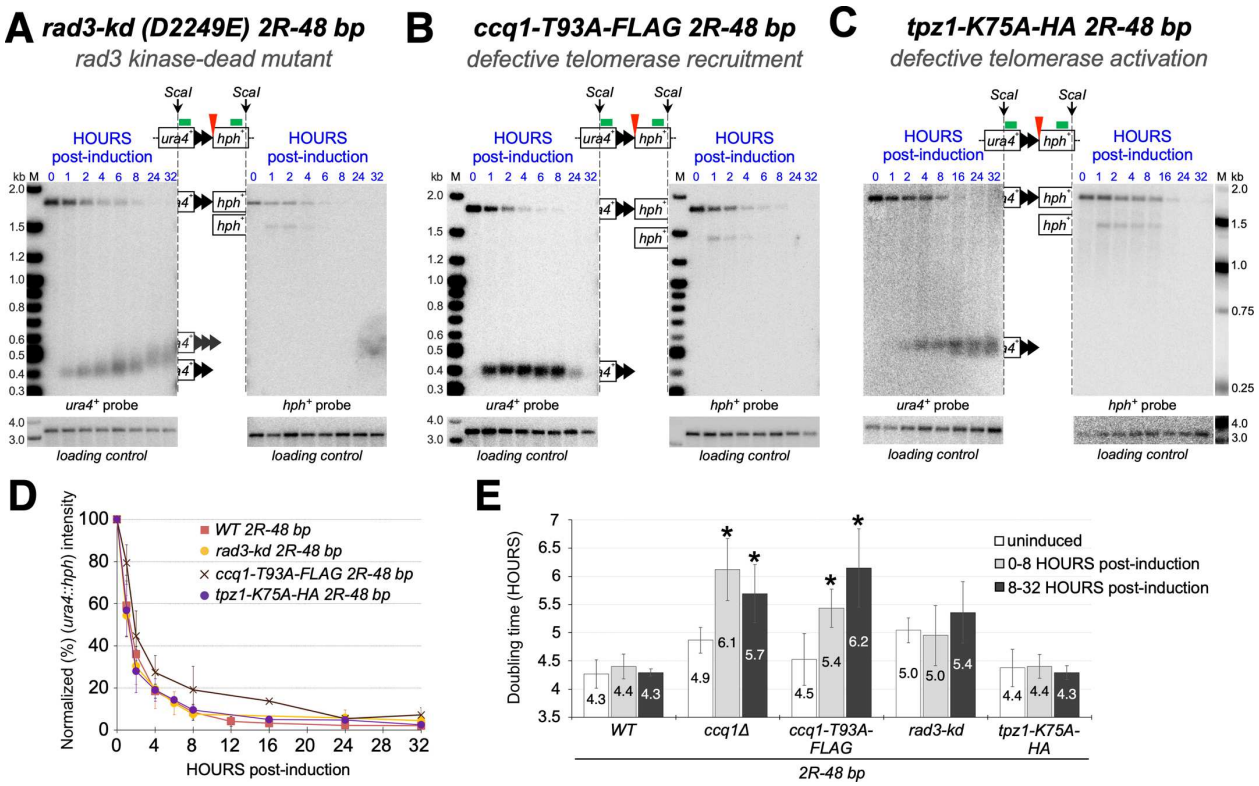

757

758 **Fig. 6. The Rad3-Ccq1 telomerase recruitment pathway is not required for the stability of**
759 **the newly formed short telomere.** *rad3-D2249E* (kinase-dead) (**A**), *ccq1-T93A* (**B**) and *tpz1-*
760 *K75A-HA* (**C**) cells bearing the *2R-48 bp* cassette were treated and analyzed as in Fig. 2B. The
761 modal terminal restriction fragment sizes of the *ura4*$^+$ cut band are presented in Table S6.
762 Additional *ccq1-T93A* and *tpz1-K75A* Southern blots are shown in Fig. S8. **(D)** Intensities
763 normalized to the loading control of the 1.8 kb uncut *ura4::hph* bands of the inductions shown in
764 A and B, derived as in Fig. 2D. Error bars are derived from two independent Southern blot
765 assays (values are in Table S1). The wild type *2R-48 bp* values from Fig. 2D are included for
766 comparison. **(E)** Doubling times of the cell cultures were determined by OD_{600nm} prior to the
767 ahTET induction (uninduced), 0-8 h post-induction and 8-32 h post-induction. Error bars show
768 standard deviations from at least three independent assays. Statistically significant differences
769 (p<0.05) are indicated by an asterisk. The wild type and *ccq1*Δ *2R-48 bp* values from Figs. 2E
770 and 4D are included for comparison.

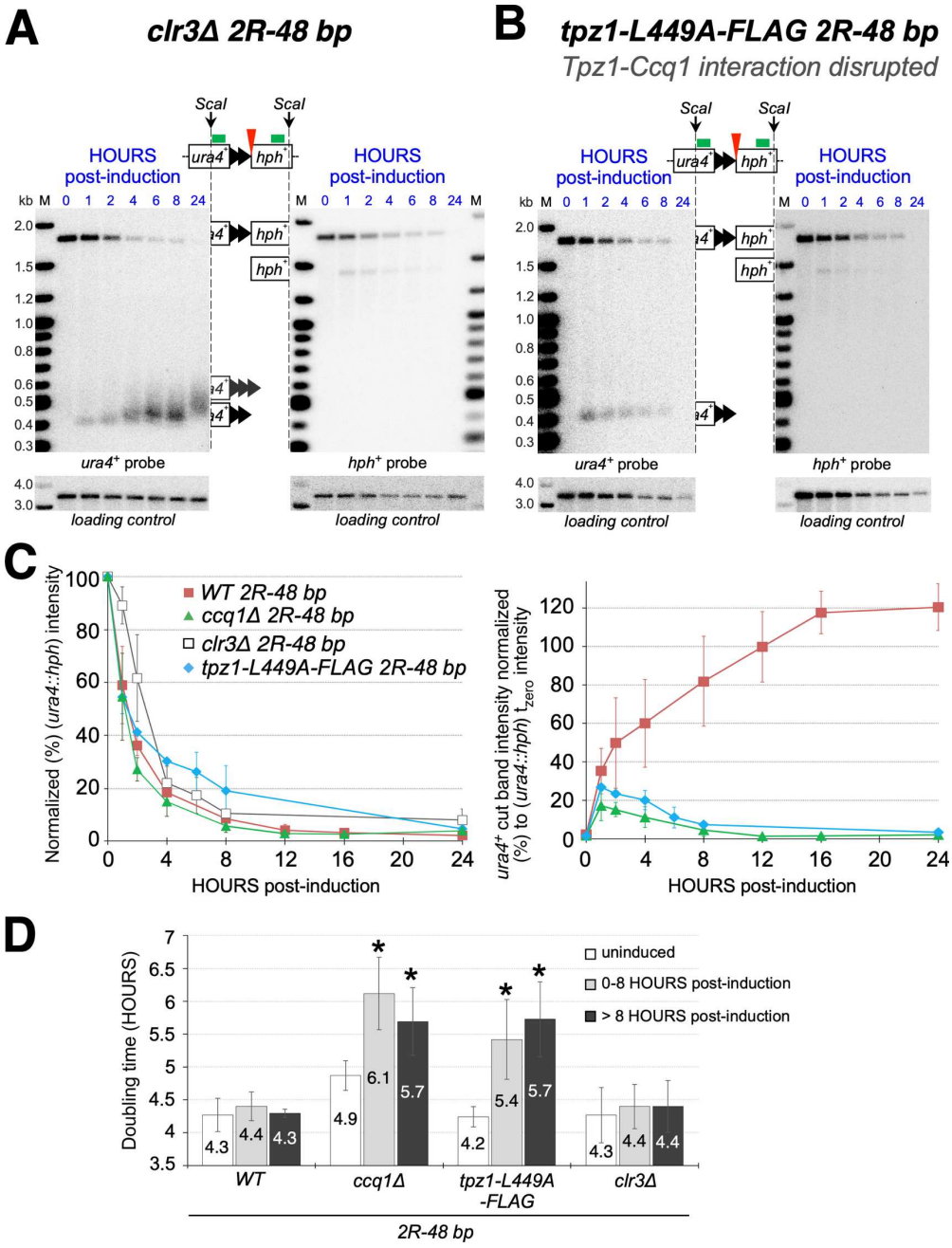

Fig. 7. The stability of the newly formed telomere requires the Ccq1-Tpz1 interaction but not Ccq1-Clr3 interaction. *clr3*Δ (**A**) and *tpz1-L449A-FLAG* (**B**) cells bearing the *2R-48 bp* cassette were treated and analyzed as in Fig. 2B. The modal terminal restriction fragment sizes of the *ura4*$^+$ cut band are presented in Table S6. An additional *tpz1-L449A* Southern blot is shown in Fig. S9. **(C) Left panel.** Intensities normalized to the loading control of the 1.8 kb uncut *ura4::hph* bands of the inductions shown in A and B, derived as in Fig. 2D. The wild type

778 and *ccq1Δ 2R-48 bp* values from Figs. 2D and 4E are included for comparison. **Right panel.**
779 Normalized intensities of the *ura4*$^+$ cut bands of the inductions shown in Fig. 2B, 4C, and 7B
780 were analyzed as in Fig. 4E. The error bars for the *tpz1-L449A 2R48 bp* strain are derived from
781 two independent Southern blots (values are in Tables S1 and S3). **(D)** Doubling times of the
782 cell cultures were determined by OD_{600nm} prior to the ahTET induction (uninduced), 0-8 h post-
783 induction, and 8-24 (> 8 h) post-induction. Error bars show standard deviations from at least
784 three independent assays. Statistically significant differences (p<0.05) are indicated by an
785 asterisk. The wild type and *ccq1Δ 2R-48 bp* values from Figs. 2E and 4D are included for
786 comparison.
787

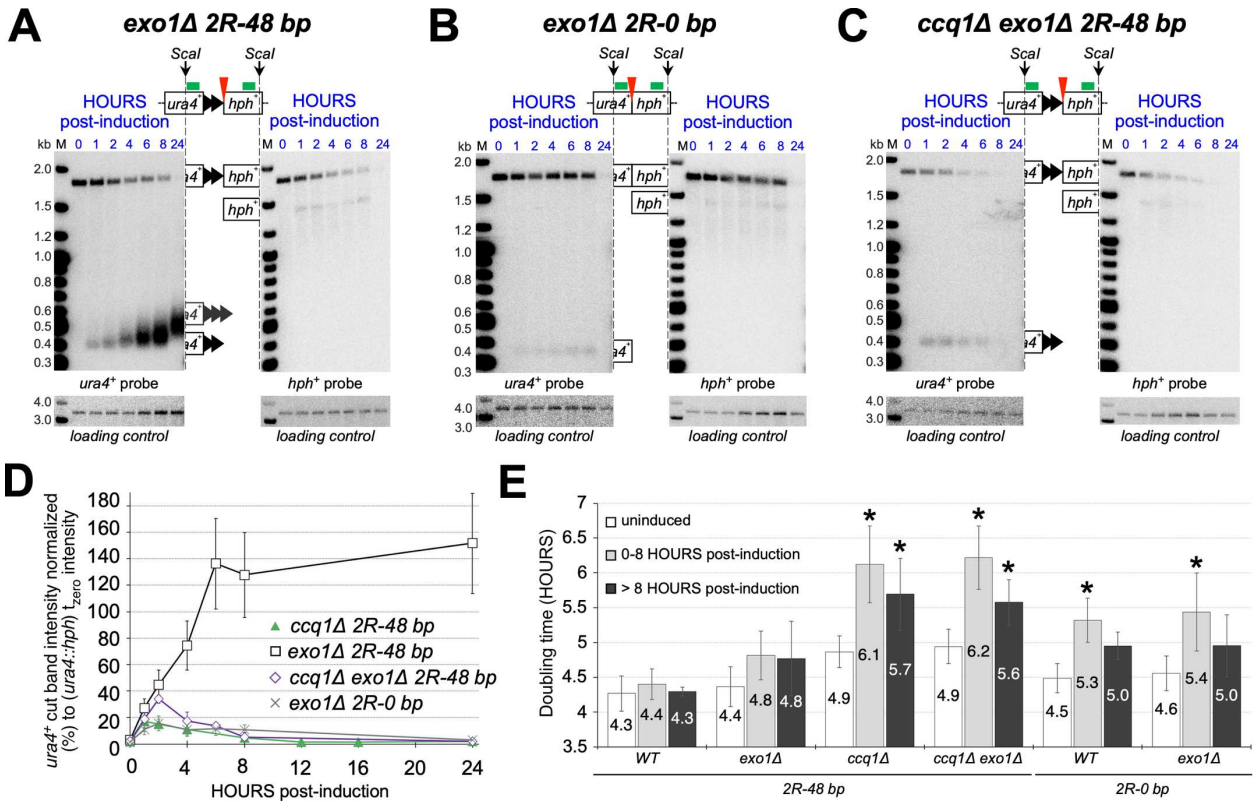

788

789 **Fig. 8. Eliminating Exo1 does not have a major effect on the newly formed short telomere**
790 **stability in *ccq1*Δ cells. (A-C)** Cells lacking Exo1 in with the indicated genotypes were treated
791 and analyzed as in Fig. 2B. The modal terminal restriction fragment sizes of the *ura4*$^+$ cut band

792 are presented in Table S6. Additional Southern blots from independent experiments are shown
793 in Fig. S10. **(D)** Normalized intensities of the *ura4*$^{+}$ cut bands of the inductions shown in Figs.
794 4C and 8A-C, were analyzed as in Fig. 4E. The error bars are derived from two independent
795 Southern blot assays for panels A and B, and three independent assays for panel C (values are
796 in Table S3). **(E)** Doubling times of the cell cultures were determined by OD_{600nm} prior to the
797 ahTET induction (uninduced), 0-8 h post-induction, and 8-24 h (>8 h) post-induction. Error bars
798 show standard deviations from at least three independent assays. Statistically significant
799 differences (p<0.05) are indicated by an asterisk. The wild type and *ccq1*Δ *2R-48 bp* values
800 from Figs. 2E and 4D are included for comparison.

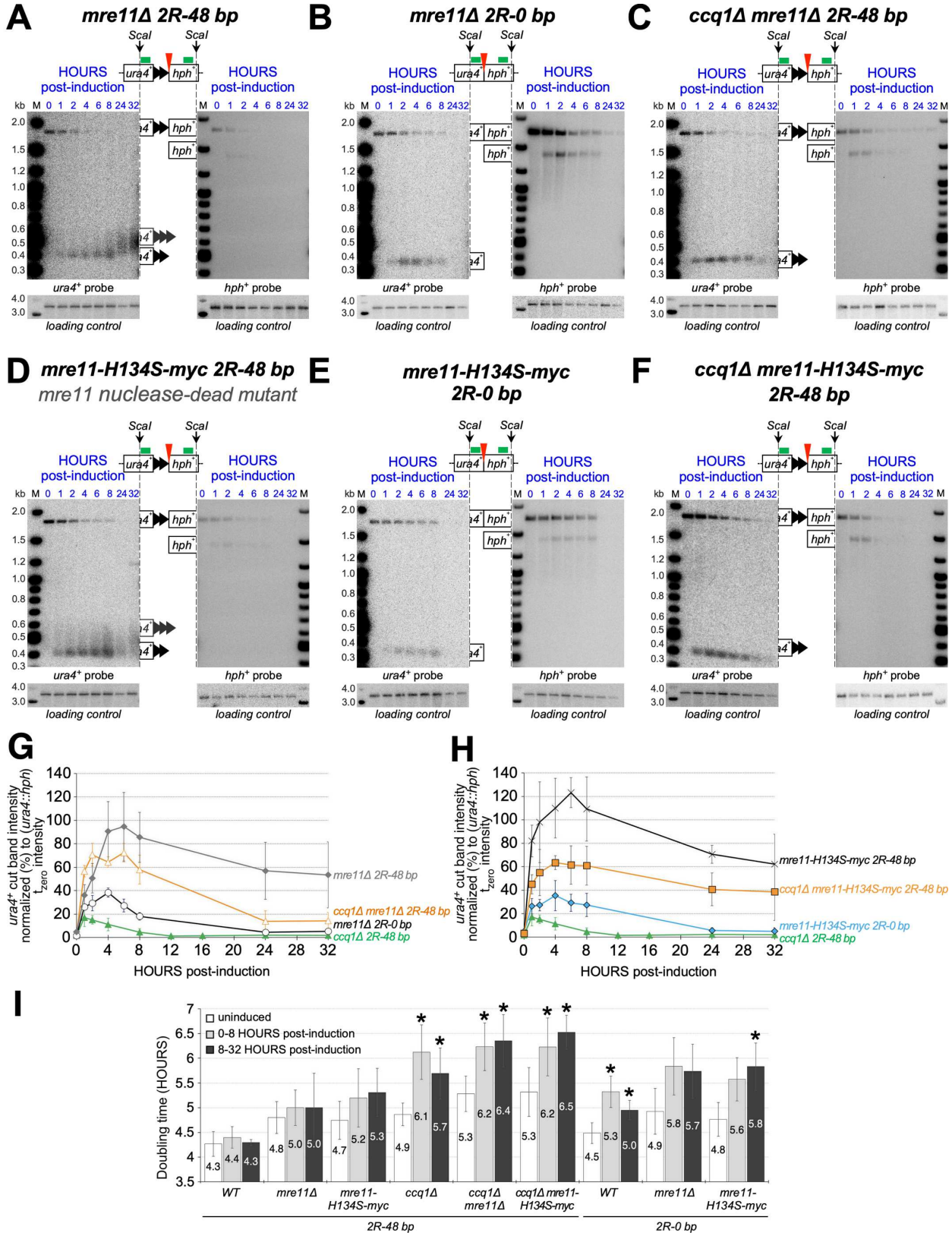
A
mre11Δ 2R-48 bp
B
mre11Δ 2R-0 bp
C
ccq1Δ mre11Δ 2R-48 bp
D
mre11-H134S-myc 2R-48 bp
mre11 nuclease-dead mutant
E
mre11-H134S-myc 2R-0 bp
F
ccq1Δ mre11-H134S-myc 2R-48 bp
ScaI
HOURS post-induction
ura4+ probe
hph+ probe
loading control
G
ura4+ cut band intensity normalized (%) to (ura4::hph) intensity tzero
HOURS post-induction
mre11Δ 2R-48 bp
ccq1Δ mre11Δ 2R-48 bp
mre11Δ 2R-0 bp
ccq1Δ 2R-48 bp
H
mre11-H134S-myc 2R-48 bp
ccq1Δ mre11-H134S-myc 2R-48 bp
mre11-H134S-myc 2R-0 bp
ccq1Δ 2R-48 bp
I
Doubling time (HOURS)
uninduced
0-8 HOURS post-induction
8-32 HOURS post-induction
WT
mre11Δ
mre11-H134S-myc
ccq1Δ
ccq1Δ mre11Δ
ccq1Δ mre11-H134S-myc
2R-48 bp
2R-0 bp

801

802 **Fig. 9. Eliminating Mre11 nuclease activity stabilizes the newly formed short telomere in**
803 ***ccq1*Δ cells.** Cells lacking Mre11 **(A-C)** or with a Mre11 nuclease dead mutant (H134S)**(D-F)**
804 with the indicated genotypes were treated and analyzed as in Fig. 2B. The modal terminal
805 restriction fragment sizes of the *ura4*$^+$ cut band are presented in Table S6. Additional Southern
806 blots from independent experiments are shown in Fig. S10. **(G)** and **(H)** Normalized intensities
807 of the *ura4*$^+$ cut bands of the inductions in *mre11*Δ strains **(G)** and *mre11-H134S* **(H)** were
808 analyzed as in Fig. 4E, and the *ccq1*Δ data from Fig. 4E is repeated for comparison. Error bars
809 are derived from two or three independent repeats of each assay (values are in Table S3). **(I)**
810 Doubling times of the cell cultures were determined by OD_{600nm} prior to the ahTET induction
811 (uninduced), 0-8 h post-induction, and 8-32 h post-induction. Error bars show standard
812 deviations from at least three independent assays. Statistically significant differences (p<0.05)
813 are indicated by an asterisk. The wild type and *ccq1*Δ *2R-48 bp* values from Figs. 2E and 4D
814 are included for comparison.
815

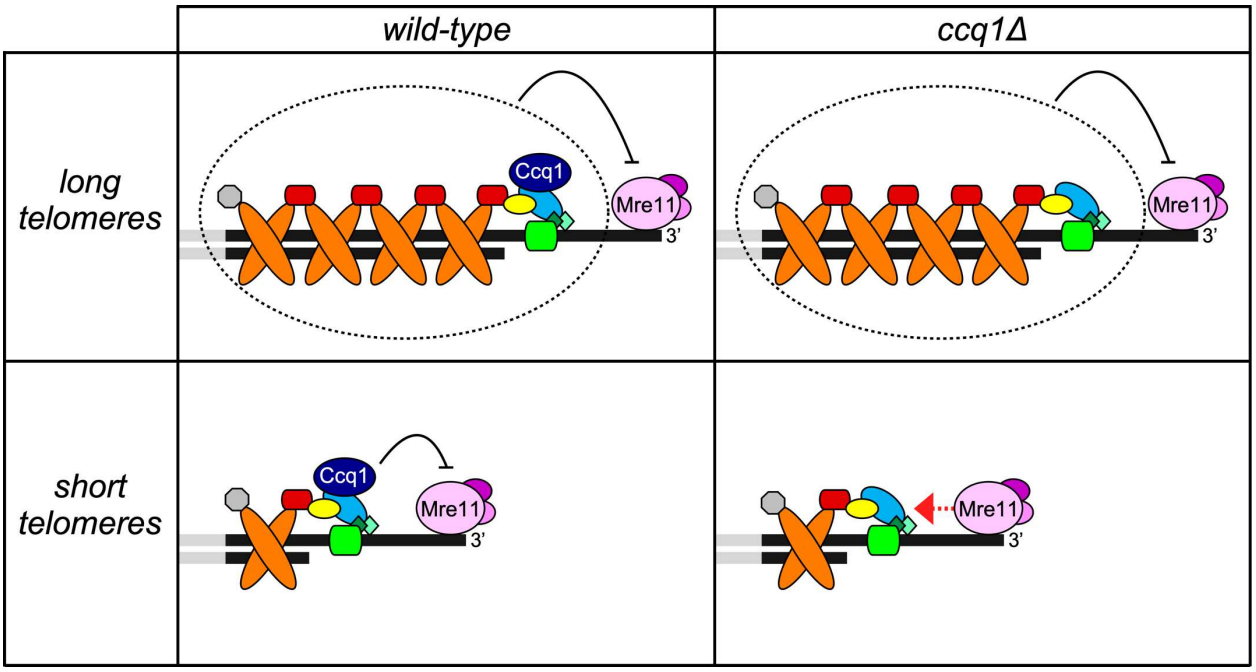

816

817 **Fig. 10. Hypothesis for the roles of Ccq1 and Taz1 in restraining Mre11 degradation of**
818 **telomeres.** Khayat et al. [56] recently identified an MRN/X inhibitory domain (called MIN) in
819 *Saccharomyces cerevisiae* Rif2 and *S. pombe* Taz1, but while mutation of this domain altered
820 *S. cerevisiae* telomeres, it had no effect on *S. pombe* telomere length or stability. Ccq1 and
821 Taz1 may therefore have redundant functions to inhibit Mre11-mediated degradation of the
822 telomere. At long telomeres in wild type cells, both Taz1 and Ccq1 act to restrain Mre11, while
823 Taz1 provides this function at long telomeres in *ccq1*Δ cells. At short telomeres (e.g. wild type
824 cells with tracts shortened by breakage), Taz1 in limiting due to the reduced number of binding
825 sites and Ccq1 restrains Mre11. When telomere repeat tracts shorten in *ccq1*Δ cells, Mre11-
826 mediated degradation occurs when the amount of Taz1 protein falls below a threshold level and
827 chromosomes either circularize or use a telomerase-independent mode of telomere replication.

Supplementary Files

This is a list of supplementary files associated with this preprint. Click to download.

- AudryRungeSI.pdf
- nrreportingsummaryAudryandRungeflatten.pdf